Unified modeling of the monotonic and cyclic behaviors of sand and clay

Yinfu Jin, Zhenyu Yin, Dong-Mei Zhang, Hong-Wei Huang

UNIFIED MODELING OF THE MONOTONIC AND CYCLIC BEHAVIORS OF SAND AND CLAY**

Yinfu Jin[1,2,3] **Zhenyu Yin**[1,2,3*] **Dongmei Zhang**[1] **Hongwei Huang**[1]

([1] *Department of Geotechnical Engineering, Tongji University, Shanghai* 200092*, China*)
([2] *Department of Civil Engineering, Shanghai Jiao Tong University, Shanghai* 200240*, China*)
([3] *LUNAM University, Ecole Centrale de Nantes, UMR CNRS GeM, Nantes* 44300*, France*)

ABSTRACT In this study, we aim to investigate a unified modeling method for the monotonic and cyclic behaviors of sand and clay. A simple double-yield-surface model, with plastic hardening modulus and dilatancy relation being dependent on density state unlike in existing approaches, is developed by considering the location of the critical state line. The model is used to simulate the drained and undrained tests of various sands and clays under monotonic and cyclic loadings. Prediction results are compared with experimental results, which show that the proposed approach is capable of modeling the monotonic and cyclic behaviors of sand and clay.

KEY WORDS sand, clay, constitutive relations, plasticity, critical state, cyclic loading

I. INTRODUCTION

Elastoplastic models based on the critical state concept proposed by Roscoe et al.[1] have been developed in the past decades to simulate the behavior of soil. Several sand models[2–4] have been built using the state parameter proposed by Been and Jefferies[5]. And several clay models[6, 7] and some viscoplastic models[8–14] also have been developed based on the original Cam-Clay model proposed by Schofield and Wroth[15] and the modified Cam-Clay model proposed by Roscoe and Burland[16]. These models can successfully capture some important features of sand or clay, but can not capture the behavior of sand and clay in an unified manner.

Given that sand and clay follow critical state theory, several unified models for the monotonic behavior of sand and clay have been developed, such as the clay and sand model (CASM)[17], the MIT-S1 model[18], and the transformed stress tensor (TS)-based model[19]. The CASM and MIT-S1 models used a special shape of the yield surface with the critical state stress ratio being larger than the stress ratio for the peak deviatoric stress. Thus, the critical deviatoric stress is smaller than the peak deviatoric stress. For normally isotropically consolidated clay, these two models can depict the strain-softening response by simulating the undrained triaxial test in compression[17, 20]. Yu et al.[21] extended the CASM to a bounding surface version to describe the cyclic behavior of sand and clay. However, the limitation of the model has not been overcome because the same yield surface is used. The TS-based model uses different critical state lines for sand and clay to avoid this limitation. This

* Corresponding author. E-mail: zhenyu.yin@gmail.com

** Project supported by the National Natural Science Foundation of China (No. 41372285), the Research Fund for the Doctoral Program of Higher Education of China (No. 20110073120012), Shanghai Pujiang Talent Plan (No. 11PJ1405700), and the European Community through the program 'People' as part of the Industry-Academia Pathways and Partnerships project CREEP (PIAPP-GA-2011-286397).

model has successfully predicted monotonic tests under special stress paths, but can not capture the cyclic tests.

In this study, we propose a unified modeling method that overcomes the aforementioned limitation and can be used to describe the monotonic and cyclic behaviors of sand and clay. Unlike existing models, the proposed model assumes that the properties of soil are dependent on the density states of sand and clay, and uses two yield surfaces to describe shear sliding and normal compression components, thus it provides an unified modeling method for sand and clay. We have incorporated a formulation similar to that used in kinematic hardening rules (i.e. Masing's rule) or the bounding surface concept, which can analyze the reverse shear loading condition, to develop a general model applicable to various stress paths, including cyclic loading.

In this study, a simple double-yield-surface model is developed by considering the density state and the location of the critical state line. First, the model is validated by simulating tests under monotonic loading. Then, the model is evaluated by comparing the predicted results with the experimental results under the cyclic loading.

II. PROPOSED MODEL FOR SAND AND CLAY

Based on elasto-plastic theory, the total strain rate is additively composed of the elastic and plastic strain rates: $\dot{\varepsilon}_{ij} = \dot{\varepsilon}^{\mathrm{e}}_{ij} + \dot{\varepsilon}^{\mathrm{p}}_{ij}$, where $\dot{\varepsilon}_{ij}$ denotes the total strain rate tensor, and superscripts e and p stand for the elastic and plastic components, respectively.

In the proposed model, the location of the critical state line and the state variable of density e_{c}/e (e_{c} is the void ratio of the critical state) were utilized. A different dilatancy relation was proposed for sand and clay within the same critical state framework.

2.1. Density State

One of the important elements that should be considered in soil modeling is the critical state concept. At the critical state, clay material retains a constant volume while it is subjected to continuous distortion. The void ratio corresponding to this state is e_{c}. The critical void ratio e_{c} is a function of the mean stress p'. The relationship between them has been expressed, with the critical state line in the e-$\log p'$ plane explicitly located by three parameters, as follows:

$$e_{\mathrm{c}} = e_{\mathrm{cr0}} - \lambda \ln\left(\frac{p'}{p_{\mathrm{cr0}}}\right) \tag{1}$$

or

$$e_{\mathrm{c}} = e_{\mathrm{cr0}} - \lambda \left(\frac{p'}{p_{\mathrm{at}}}\right)^{\xi} \tag{2}$$

where e_{cr0} and p_{cr0} determine the reference critical state in the e-$\log p'$ plane, and λ determines the slope of the critical state line. Alternatively, a reference value of e_{cr0}, with two constants λ and ξ based on the assembly of critical state points, is used to determine the critical state line. For convenience, the value of p_{cr0} is assumed to equal to the reference pressure p_{ref} for the reference void ratio (see Fig.4(a)). Then, the critical state line can be defined by two parameters, e_{cr0} and λ, when using Eq.(1). Alternatively, a nonlinear function, i.e., Eq.(2), is used for sand based on the assembly of critical state points. Using the critical state concept, the density state of soil is defined as ratio e_{c}/e, where e is the void ratio of soil.

2.2. Elastic Behavior

The elastic behavior of sand and clay is assumed to be isotropic, which is similar to the sand model, as follows:

$$\dot{\varepsilon}^{\mathrm{e}}_{ij} = \frac{1+\upsilon}{E}\dot{\sigma'}_{ij} - \frac{\upsilon}{E}\dot{\sigma'}_{kk}\delta_{ij} \tag{3}$$

where υ and E are Poisson's ratio and Young's modulus, respectively; σ'_{ij} is the effective stress tensor; and δ_{ij} is Kronecker's delta. E can also be replaced by elastic bulk modulus K, as follows: $E = 3K\,(1-2\upsilon)$. The elastic bulk modulus is defined as follows:

$$K = K_0 \left(\frac{p'}{p_{\mathrm{at}}}\right)^{n} \tag{4}$$

where K_0 and n are the soil constants, $p' = (\sigma'_1 + \sigma'_2 + \sigma'_3)/3 = \sigma'_{ii}/3$ is the mean effective stress, and p_{at} is the atmospheric pressure used as the reference pressure ($p_{at} = 101.325$ kPa). For sand, the value of n is approximately 0.5 to 0.6. For clay, K_0 can be estimated from the slope of swelling line κ and initial void ratio e_0, as follows: $K_0 = p_{at}\,(1 + e_0)/\kappa$, with $n = 1$.

Elastic shear stiffness G is related to elastic bulk modulus K through Poisson's ratio υ:

$$G = \frac{3\,(1 - 2\upsilon)}{2\,(1 + \upsilon)} K \tag{5}$$

2.3. Plastic Behavior

The proposed approach uses two yield surfaces for the shear sliding and normal compression components (see Fig.1). Thus, the framework of the proposed approach is similar to that of the double-hardening or double-yield-surface models[22, 23]. However, the density state and the location of the critical state line are used in the constitutive equations for clay.

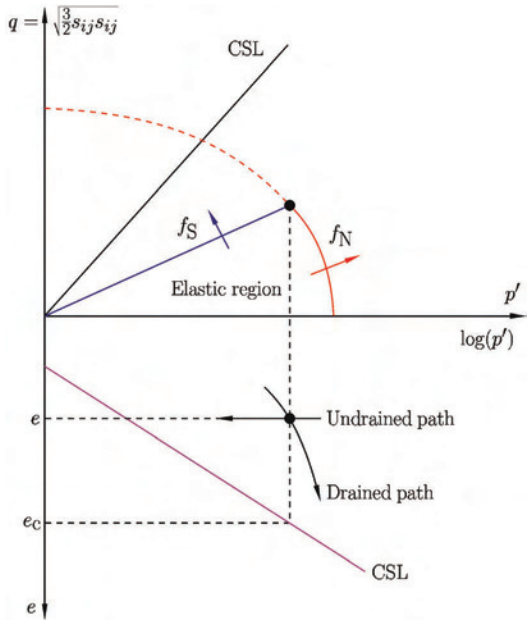

Fig. 1. Principle of the simple density state model for sand and clay.

Based on conventional elasto-plastic theory, the plastic strain can be obtained by using the equation: $\dot{\varepsilon}^{\mathrm{p}}_{ij} = \Lambda \cdot \partial g / \partial \sigma'_{ij}$, where Λ is the plastic multiplier that depends on the stress rate and the plastic hardening law, and g is the plastic potential.

2.3.1. Shear sliding criterion

As observed from many sand models[2, 3, 22, 24], the shape of the yield surface for the shear component is linear in the p'-q plot. In this approach, we adopt the shear criterion of sand for clay can be written as follows:

$$f_S = \sqrt{\frac{3}{2} r_{ij} r_{ij}} - H \tag{6}$$

where $r_{ij} = s_{ij}/p'$, $s_{ij} = \sigma'_{ij} - p'\delta_{ij}$ with δ_{ij} denoting the Kronecker delta, and H is the hardening parameter defined by a hyperbolic function in the H-$\varepsilon^{\mathrm{p}}_{\mathrm{d}}$ plane, which is given as follows:

$$H = M_{\mathrm{p}} \frac{G_{\mathrm{p}} K \varepsilon^{\mathrm{p}}_{\mathrm{d}}}{M_{\mathrm{p}} p' + G_{\mathrm{p}} K \varepsilon^{\mathrm{p}}_{\mathrm{d}}} \tag{7}$$

where G_{p} is used to control the initial slope of the hyperbolic curve η-$\varepsilon^{\mathrm{p}}_{\mathrm{d}}$ ($\eta = q/p'$, with q representing the deviatoric stress, and $\eta = \sqrt{3 r_{ij} r_{ij}/2}$ in the general stress space). Equations (6) and (7) guarantee

that the current stress ratio is equivalent to the peak critical state value M_{p}, which is associated with the peak strength of the materials during plastic shear straining (e.g., in the case of triaxial shearing). Thus, a nonlinear shear stress–strain relationship can be reproduced.

According to Biarez and Hicher[25], the maximum frictional angle ϕ_{p} (associated with M_{p} by the expression $M_{\mathrm{p}} = 6\sin\phi_{\mathrm{p}}/(3-\sin\phi_{\mathrm{p}})$), the intrinsic friction angle ϕ_{μ} (associated with the critical state value by the expression $M = 6\sin\phi_{\mu}/(3-\sin\phi_{\mu})$), and the density state of soil (e_{c}/e) satisfy the following equation:

$$e\tan\phi_{\mathrm{p}} = e_{\mathrm{c}}\tan\phi_{\mu} = \text{Constant} \tag{8}$$

Equation (8) can be adopted to describe the shear behavior of sand and clay, which indicates that the maximum frictional angle ϕ_{p} is smaller than ϕ_{μ} in a loose structure. By contrast, a dense structure provides a high degree of interlocking. Thus, the maximum frictional angle ϕ_{p} is greater than ϕ_{μ}. When loading stress reaches the maximum frictional angle ϕ_{p}, the dense structure dilates and the degree of interlocking decreases. Consequently, the maximum frictional angle is reduced, which results in a strain-softening phenomenon. Notably, Eq.(8) has been successfully applied in micromechanics-based models[26–37]. M_{p} can be obtained using Eq.(8). We interpolated M within the range from M_{c} (for compression) to M_{e} (for extension in the general stress space by means of the lode angle θ[38], which is expressed as follows:

$$M = M_{\mathrm{c}}\left[\frac{2c^4}{1+c^4+(1-c^4)\sin(3\theta)}\right]^{1/4} \tag{9}$$

where $c = M_{\mathrm{e}}/M_{\mathrm{c}}$, $-\pi/6 \le \theta = \sin^{-1}\left[-3\sqrt{3}J_3/\left(2J_2^{3/2}\right)\right]/3 \le \pi/6$. J_2 and J_3 are the second and third invariants of a deviator stress tensor, which are given as $J_2 = s_{ij}s_{ij}/2$ and $J_3 = s_{ij}s_{jk}s_{ki}/3$, respectively. In this study, we assume that the frictional angles for compression and extension are the same, i.e., $c = (3-\sin\phi_{\mu})/(3+\sin\phi_{\mu})$.

G_{p} is assumed to be a function of the relative density D_{r} of sand and the overconsolidation ratio OCR of clay as follows:

$$G_{\mathrm{p}} = \begin{cases} G_{\mathrm{p0}}\exp\left(h_1 D_{\mathrm{r}}\right) & -\text{Sand} \\ G_{\mathrm{p0}}\mathrm{OCR}^{h_1} & -\text{Clay} \end{cases} \tag{10}$$

where G_{p0}, h_1, and h_2 are the soil constants; $D_{\mathrm{r}} = (e_{\max}-e)/(e_{\max}-e_{\min})$, with e as the current void ratio, $e_{\min}$ as the minimum void ratio, and $e_{\max}$ as the maximum void ratio of sand; $\mathrm{OCR} = p_{\mathrm{c\_d}}/p_{\mathrm{c}}$, with $p_{\mathrm{c\_d}}$ being the size of the surface that passes through the current stress state and p_{c} being the size of the yield surface that corresponds to the current stress state. The yield surface for clay is presented in a later section.

We propose a dilatancy equation using the density state to consider dilation or contraction during shear sliding. The dilatancy equation for sand and clay is given as follows:

$$\frac{\mathrm{d}\varepsilon_{\mathrm{v}}^{\mathrm{p}}}{\mathrm{d}\varepsilon_{\mathrm{d}}^{\mathrm{p}}} = \begin{cases} D_a\left(M_{\mathrm{pt}}-\eta\right)\exp\left[h_2\left(\dfrac{e}{e_{\mathrm{c}}}-1\right)\right] & -\text{Sand} \\ D_a\left|M-\eta\right|\left(\dfrac{\eta}{M}\right)^{D_b}\left(\dfrac{e}{e_{\mathrm{c}}}-1\right) & -\text{Clay} \end{cases} \tag{11}$$

where D_a and D_b are the soil constants, and M_{pt} is the slope of the phase transformation line for sand, which can be derived from frictional angle ϕ_{μ} by using the equation: $e\tan\phi_{\mathrm{pt}} = e_{\mathrm{c}}\tan\phi_{\mu}$.

The proposed equation allows more flexibility to model different types of clay behavior. Constants D_a and D_b control the magnitude and evolution of dilatancy, respectively. The term $(e_{\mathrm{c}}/e-1)$ is used to regulate dilation or contraction for the normally or slightly consolidated state ($e > e_{\mathrm{c}}$) contraction and the heavily overconsolidated state ($e < e_{\mathrm{c}}$) dilation. When stress state reaches the critical state line, void ratio e is equal to critical void ratio e_{c}, which induces $M_{\mathrm{pt}} = \eta$. With η reaching critical state M, zero dilation or contraction holds. Thus, the equation guarantees that stresses and void ratios simultaneously reach the critical state line in the p'-q-e plane.

2.3.2. Normal compression criterion

A second yield surface is added to describe the compression behavior of clay. The second yield function is assumed as follows:

$$f_{\mathrm{N}} = p'^2 + \frac{3}{2}\frac{s_{ij}s_{ij}}{R^2} - p_{\mathrm{c}}^2 \tag{12}$$

where constant R controls the shape of the yield surface and p_c is the hardening parameter that controls the size of the yield surface. The yield surface expands with the plastic volumetric strain. The hardening rule of the modified Cam-Clay model is adopted, i.e.,

$$\mathrm{d}p_c = p_c \frac{1+e_0}{\lambda-\kappa}\mathrm{d}\varepsilon_v^p \tag{13}$$

Given that initial elastic modulus K_0 is used as input, κ is obtained using the equation: $\kappa = p_{at}(1+e_0)/K_0$. The associated flow rule is adopted for normal compression.

Parameter Rcan be derived as follows:

For the 1D strain case:

$$\frac{\mathrm{d}\varepsilon_d}{\mathrm{d}\varepsilon_v} = \frac{2}{3} \tag{14}$$

Assuming that elastic strains are smaller than plastic strains, Eq.(14) can be approximated using the following equation:

$$\frac{\mathrm{d}\varepsilon_d^p}{\mathrm{d}\varepsilon_v^p} = \frac{2}{3} \tag{15}$$

Combining Eq.(15) with the flow rule derived from Eq.(12) (i.e., $\mathrm{d}\varepsilon_d^p = \Lambda \cdot \partial f_N/\partial q$, $\mathrm{d}\varepsilon_v^p = \Lambda \cdot \partial f_N/\partial p$), we can express the consolidation R for the 1D case as follows:

$$R = \sqrt{\frac{3}{2}\eta_{K0}} \tag{16}$$

where $\eta_{K0} = 3M/(6-M)$ for normally consolidated clay by adopting Jacky's formula.

2.4. Stress Reversal Technique

The direction of shear sliding is reversed upon shear reversal. We denote the stress state at the moment of shear reversal as the residual stress, which significantly influences subsequent shear behavior. Consequently, the hardening rule and the dilation can be derived using the following equations:

$$H = M_p^* \frac{G_p K \varepsilon_d^{p*}}{M_p^* p' + G_p K \varepsilon_d^{p*}} \tag{17}$$

$$\frac{\mathrm{d}\varepsilon_v^p}{\mathrm{d}\varepsilon_d^p} = \begin{cases} D_a\left(M_{pt}^* - \eta^*\right)\exp\left[h_2\left(\dfrac{e}{e_c}-1\right)\right] & -\text{Sand} \\ D_a\left|M^* - \eta^*\right|\left(\dfrac{\eta^*}{M^*}\right)^{D_b}\left(\dfrac{e}{e_c}-1\right) & -\text{Clay} \end{cases} \tag{18}$$

Note that these two equations have the same form as the previous equations. The only difference is the superscript (*) marked on the plastic shear strain ε_d^{p*}, the mobilized stress ratio η^*, the critical state stress ratio M^*, the peak stress ratio M_p^*, and the phase transformation stress ratio M_{pt}^*, which are defined in the following equations to show the effect of the reverse state (see Fig.2):

$$\varepsilon_d^{p*} = \sqrt{\frac{2}{3}\left(e_{ij}^p - e_{ij}^{pR}\right)\left(e_{ij}^p - e_{ij}^{pR}\right)} \tag{19}$$

$$\eta^* = \eta_R - \eta \tag{20}$$

$$M^* = \eta_R - M, \qquad M_p^* = \eta_R - M_p, \qquad M_{pt}^* = \eta_R - M_{pt} \tag{21}$$

where $e_{ij} = \varepsilon_{ij} - \varepsilon_v \delta_{ij}/3$, η_R is the mobilized stress ratio at the moment of stress reversal, and e_{ij}^{pR} is the plastic deviatoric strain tensor at the moment of stress reversal. η_R and η are positive when the stresses applied to the sample are in a compression state and negative when the stresses applied to the sample are in an extension state (in Fig.2(b), η represents distance). The value of M is positive when the applied incremental stresses are in a compression state, and vice versa.

Equation (18) indicates that the dilation amount is different upon shear reversal. This concept is similar to that proposed by Balendran and Nemat-Nasser[39] and Wan and Guo[40]. Equation (17) indicates that the same form of hardening rule can be used for loading and unloading conditions, but may require some scaling processes on the values of M_p. This concept is similar to that used in Masing's rule and in bounding surface plasticity[41].

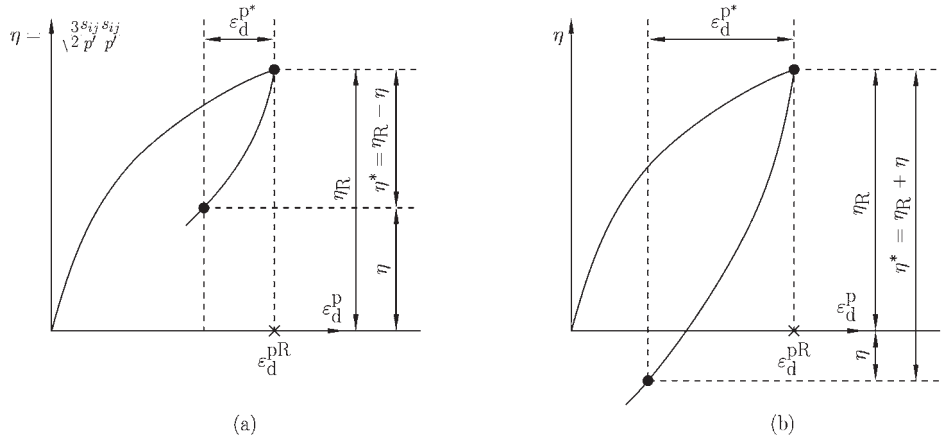

Fig. 2. Principle of stress reversal in loading and unloading.

2.5. Model Parameters

Based on all the aforementioned constitutive equations, the proposed model involves 13 parameters, which can be divided into 4 groups for the sand, and 11 parameters with 1 additional group for the clay, as listed in Table 1. Given that the physical interpretation of all parameters is clear, as presented in the previous sections, model parameters can be easily determined. An example is given in the following section.

Table 1. **Index properties of clay samples and locations of critical state for undrained test**

Group	Parameter	Definition	Nevada sand	Toyoura sand	Kaolin clay[1]	Kaolin clay[2]	Black clay	LCT	Clay mixture
Elasticity	K_0	Bulk modulus	20000	20000	6080	9200	3000	19250	6170
	n	Nonlinear elastic constant	0.6	0.5	–	–	–	–	–
	υ	Poisson's ratio	0.2	0.2	0.2	0.2	0.2	0.2	0.2
	e_0	Initial void ratio	–	–	2.05	2.17	1.34	0.52	1.07
Critical state	M_{c}	Slope of the critical state line in compression	1.3	1.27	0.9	0.89	0.83	1.2	0.75
	e_{cr0}	Reference critical void ratio for compression	0.79	0.934	2.21	2.04	1.33	0.587	0.975
	p_{cr0}/ξ	Reference critical state stress/nonlinear constant for sand	0.7	0.7	10	100	100	10	100
	λ	Slope of the critical state line in the e-log p' plane	0.015	0.019	0.26	0.18	0.244	0.066	0.173
Plastic hardening	G_{p0}	Initial slope of the curve η-ε_d^p	15	2	2.3	0.35	10	1.3	0.5
	e_{min}	Minimum void ratio for sand	0.5	0.60	–	–	–	–	–
	e_{max}	Maximum void ratio for sand	0.9	0.98	–	–	–	–	–
	h_1	Plastic hardening parameter	1	3	0.5	4	0.5	0.5	1
Dilatancy	D_a	Constant to control the magnitude of dilatancy	5	1	10	30	40	7	1.7
	D_b	Constant to control the evolution of dilatancy for clay	–	–	0.5	0.5	2	0.3	0.1
	h_2	Dilatancy parameter for sand	13	3	–	–	–	–	–
Compression	p_{c0}	Initial size of yield surface for clay	–	–	50	100	165	75	100

Remark: Kaolin clay[1] (Wroth and Loudon, 1967); kaolin clay[2] (Al-Tabbaa, 1987).

III. EXPERIMENTAL VERIFICATION

Experimental verification is presented in this section, with reference to drained and undrained tests on the sand and clay under monotonic and cyclic loadings. The test results for Nevada and Toyoura sand were compared with the simulation results to validate the proposed method for the sand. In parallel, the test results for kaolin clay, black clay, Lower Cromer Till (LCT), and clay mixture were compared

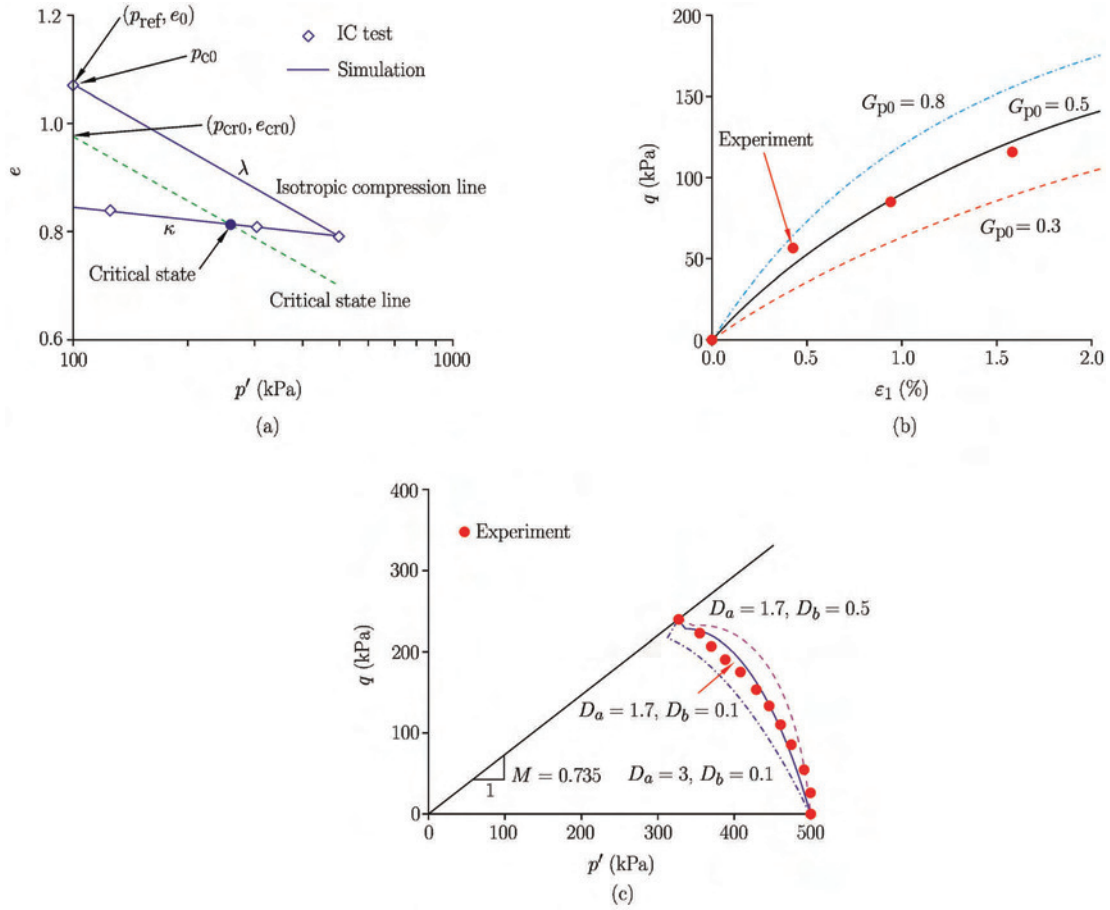

Fig. 3. The calibration of model parameters.

with the simulation results to validate the proposed model for the clay.

3.1. Calibration of Model Parameters

Two undrained compression tests with different OCRs and an isotropic consolidation test are required to calibrate model parameters. The tests on clay mixture conducted by Li and Meissner[42] were selected as an example for the calibration procedure, as shown in Fig.3. The details of the test and the clay used will be presented later in this section. Figure 3(a) is plotted using the experimental data provided by Li and Meissner[42]. Parameters e_0, e_{cr0_c}, p_{c0}, ρ, κ, and λ (see Table 1) can be obtained from the isotropic consolidation curve (see Fig.3(a)). The slope of critical state line M was measured from the undrained triaxial test (see Fig.3(c)). Other parameters can be obtained by the curve fitting (as shown in Figs.3(a) to (c)), as follows:

(1) Shear hardening parameter G_{p0} was determined from the q-ε_1 curve of the undrained compression test at the small strain level by the curve fitting, as shown in Fig.3(b).

(2) Dilation constants D_a and D_b were determined from the undrained compression test by the curve fitting (see Fig.3(c), which is similar to that for sand). Notably, the undrained stress path varies with different values of D_a and D_b, which implies that the proposed dilatancy flow rule can describe different shapes of the yield surface.

(3) Plastic hardening parameter h_1 was determined from the slope of the q-ε_1 curve of the undrained test, with OCR = 4 (Fig.4(a)).

(4) The initial value of the size of yield surface p_{c0} (see Eq.(12)) was determined based on stress history.

The determined values of the model parameters were used to simulate undrained triaxial tests with different OCRs. As shown in Fig.4, good agreement was achieved between the model predictions and

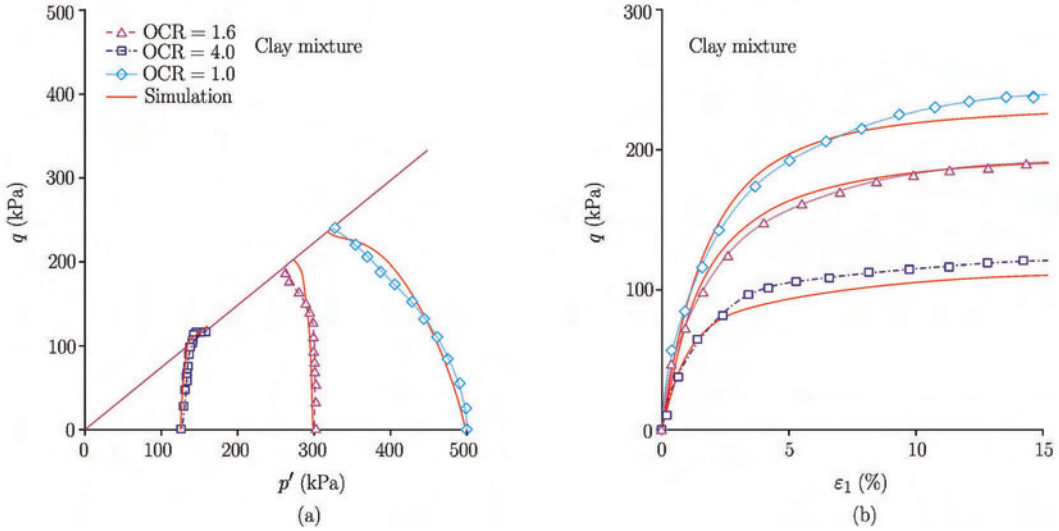

Fig. 4. Comparison between the experimental and numerical results for undrained triaxial compression tests on clay mixture with OCR from 1 to 4.

the experimental results. Therefore, the model determination procedure was validated. The simulation results for the undrained tests on the same clay under cyclic loading will be presented later.

For sand, K_0 and n can be determined through the isotropic compression test or the odometer test. Alternatively, K_0 and n can be calibrated from the initial slope of the q-ε_1 curve under different confining stress levels. Other parameters can be determined in the same manner as that for clay. All determined parameters for sand and clay are summarized in Table 1.

3.2. Monotonic Modeling for Sand

3.2.1. Nevada sand

Laboratory tests conducted on Nevada sand[43] were used to validate the model. Nevada sand ($D_{50} = 0.15$ mm) has a maximum dry density of 17.33 kN/m^3 ($e_{\min} = 0.5$), a minimum dry density of 3.87 kN/m^3 ($e_{\max} = 0.9$), and a specific gravity of 2.67. Monotonic triaxial tests with different densities and confining pressures under drained and undrained loading conditions are available. Drained tests were conducted under constant confining pressures. The tests were mainly performed on samples with relative densities (D_{r}) of 40% and 60% under confining pressures of 40, 80, and 160 kPa. The void ratios that correspond to $D_{\mathrm{r}} = 40\%$ and 60% are 0.74 and 0.66, respectively.

The critical state line was measured from the critical states in the e-$\log p'$ plane (Fig.5(a)). Other parameters were measured and determined from the drained tests based on the aforementioned procedure and summarized in Table 1. Notably, dilatancy constant D_a was determined from the e-ε_1 curve instead of from the undrained stress path.

Figure 6 shows the stress–strain and volumetric responses of drained compression tests for Nevada sand with $D_{\mathrm{r}} = 40\%$ (Figs.6(a) and (b)) and 60% (Figs.6(c) and (d)). Good agreement with the experimental results is achieved at both densities and for different confining pressures. The simulation and experimental results show that dense sand has a stiffer hardening response, higher peak value, and larger dilation compared with loose sand. Dense sands also exhibit a more pronounced softening that follows the peak deviatoric stress.

The same values of the model parameters were used to simulate an undrained compression test conducted on samples of the same Nevada sand with a void ratio of 0.66. The model predictions and the conventional undrained compression test results are shown in Fig.7. In general, the test results and model simulation results are in good agreement.

3.2.2. Toyoura sand

Toyoura sand is uniform fine quartzitic sand that consists of sub-rounded to sub-angular particles, which is the standard cohesionless soil[44–47]. Toyoura sand has a maximum void ratio of 0.977, a minimum

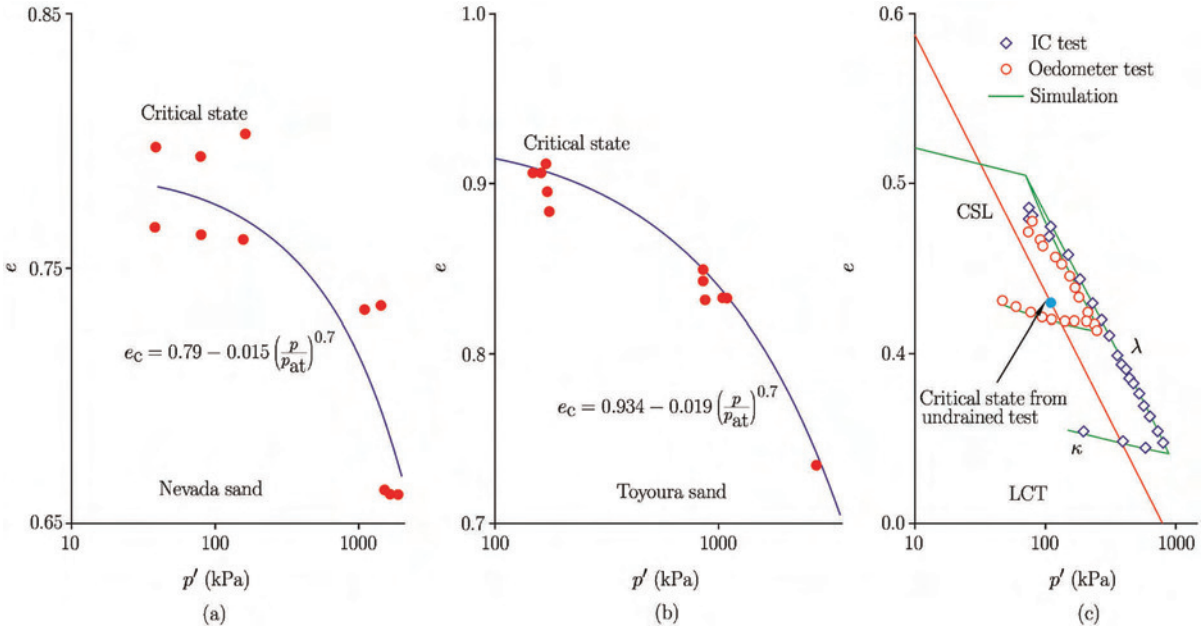

Fig. 5. Critical state line for (a) Nevada sand, (b) Toyoura sand, and (c) compression and critical state line for LCT.

void ratio of 0.597, and a specific gravity of 2.65. Verdugo and Ishihara[44] conducted a complete set of monotonic drained and undrained triaxial tests on isotropically consolidated samples of Toyoura sand with a mean diameter $D_{50} = 0.17$ mm and a uniformity coefficient $C_u = 1.7$. These tests have been conducted under an extensive range of void ratios and confining pressures: (1) drained triaxial tests with void ratios ranging from 0.810 to 0.996 under constant lateral stress of 100 kPa and 500 kPa, and (2) undrained triaxial tests with void ratios ranging from 0.735 to 0.907 under different confining pressures from 0.1 MPa to 3 MPa.

The critical state line was measured from the critical states in the e-log p' plane (Fig.5(b)). Other parameters were measured and determined from the undrained tests based on the aforementioned procedure and summarized in Table 1.

Figure 8 shows the comparison between experimental data and the simulation results of isotropically consolidated samples under undrained triaxial compression. Figure 9 shows the comparison between the data and the simulation results of isotropically consolidated samples of the same Toyoura sand under the drained triaxial compression. The tests cover an extensive range of confining pressures and void ratios, where very loose, loose, and medium sand are considered. The comparison between the test results and model predictions shows good agreement.

3.3. Monotonic Modeling for Clay

3.3.1. Pure clay

Undrained triaxial tests on saturated kaolin conducted by Wroth and Loudon[48] and drained triaxial tests on black clay conducted by Biarez and Hicher[25] were used to evaluate model applicability in the pure clay. The selected tests were performed on kaolin specimens with isotropic consolidation under different OCRs from 1 to 6.5 for undrained tests and from 1 to 8 for drained tests. Model parameters were determined from undrained tests for kaolin clay and from drained tests for black clay. The values are summarized in Table 1.

Figure 10 shows the comparison between the measured and predicted results for undrained tests. It can be seen from Fig.10 that the predicted undrained stress paths can describe the behavior of clay and the proposed model provides excellent predictions for tests on all lightly and heavily overconsolidated samples. In addition, Fig.11(d) shows the predicted undrained paths, including the consolidation stages, in the e-log p' plane for samples with various OCRs, which is a typical undrained path for clay, as observed in the experiments. The simulated undrained paths are derived using the constitutive equations.

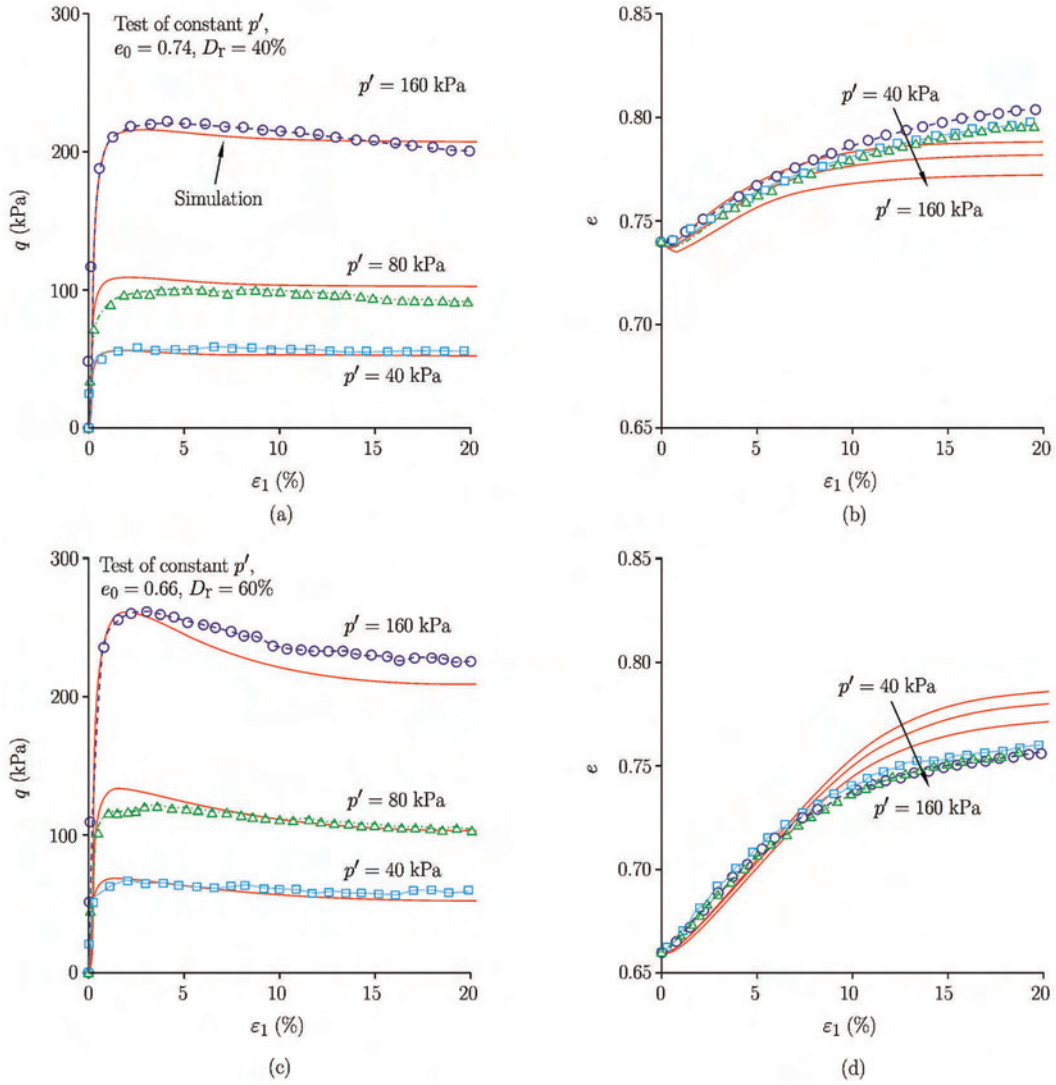

Fig. 6. Comparison between the experimental and numerical results for p'-constant drained triaxial compression tests of Nevada sand.

Figure 11 shows the comparison between the measured and predicted results for drained tests. The model describes the general drained behavior of clay, but provides poor predictions on all lightly and heavily overconsolidated samples. In addition, Fig.11(c) shows the predicted and experimental drained paths, including the consolidation stages, in the e-log$\,p'$ plane for samples with various OCRs. The simulated drained paths are derived using the constitutive equations.

3.3.2. LCT

Undrained triaxial tests in compression and extension with different OCRs on anisotropically consolidated samples of LCT were conducted by Gens[49]. LCT, which is classified as a low plasticity silty clay, has a liquid limit $w_L = 25\%$ and a plasticity index $I_p = 13\%$. The tests on LCT were all conducted on specimens consolidated from a slurry with an initial water content $w = 31\%$. Model parameters were determined from the undrained tests with an isotropic consolidation test (Fig.5(c)) and summarized in Table 1.

Simulations were also conducted to evaluate the performance of the model in predicting the compression and extension tests on anisotropically consolidated samples (Fig.12). First, the samples were anisotropically consolidated under $K_0 = 0.5$ up to $\sigma'_a = 350$ kPa. Then, the samples were unloaded along a different stress path with four different OCRs (OCR = 1, 2, 4, 7) before undrained shearing was

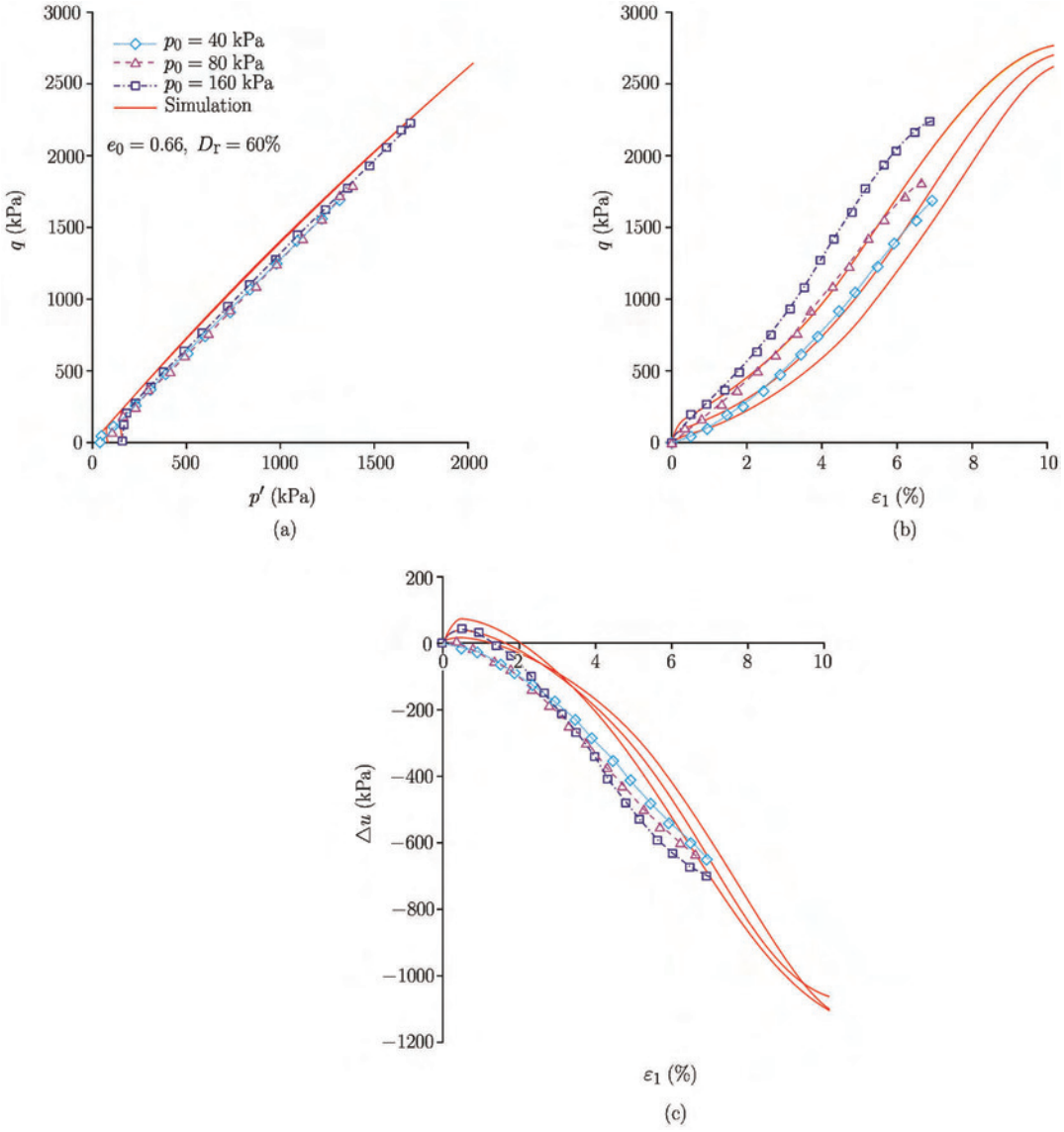

Fig. 7. Comparison between the experimental and numerical results for undrained triaxial compression tests of Nevada sand.

performed in compression and extension. Figure 12 gives the comparison between the experimental data and the model predictions, which indicates good agreement in the major features of the undrained behavior of anisotropic samples. However, the predicted shear strengths of the compression tests (OCR = 4, 7) are lower than those from the experimental results (see Fig.12(b)).

Figure 13 shows the comparison between the experimental data and the model predictions for drained anisotropic specimens with different OCRs. Similar to the undrained tests, the samples were first anisotropically consolidated with $K_0 = 0.5$, and then unloaded to different values of OCR (1, 1.5, 2, 4, and 7) through a different stress path. Subsequently, the axial load of the samples increased until the vertical strain reached 15%. The trends of shear strength and volume change of the samples with different OCR values were also reproduced by the proposed model using the same set of parameters for undrained tests.

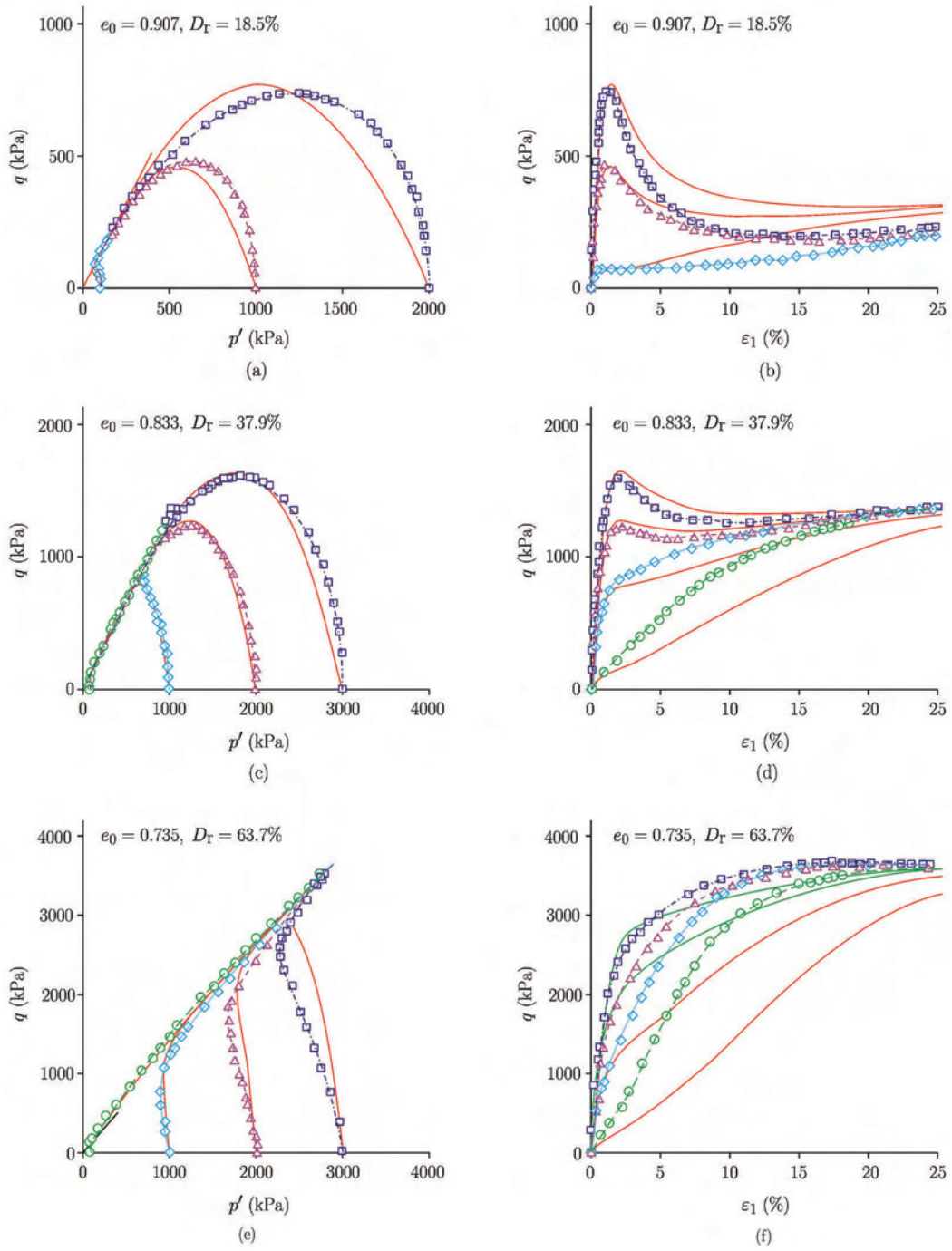

Fig. 8. Comparison between the experimental and numerical results for undrained triaxial compression tests of Toyoura sand.

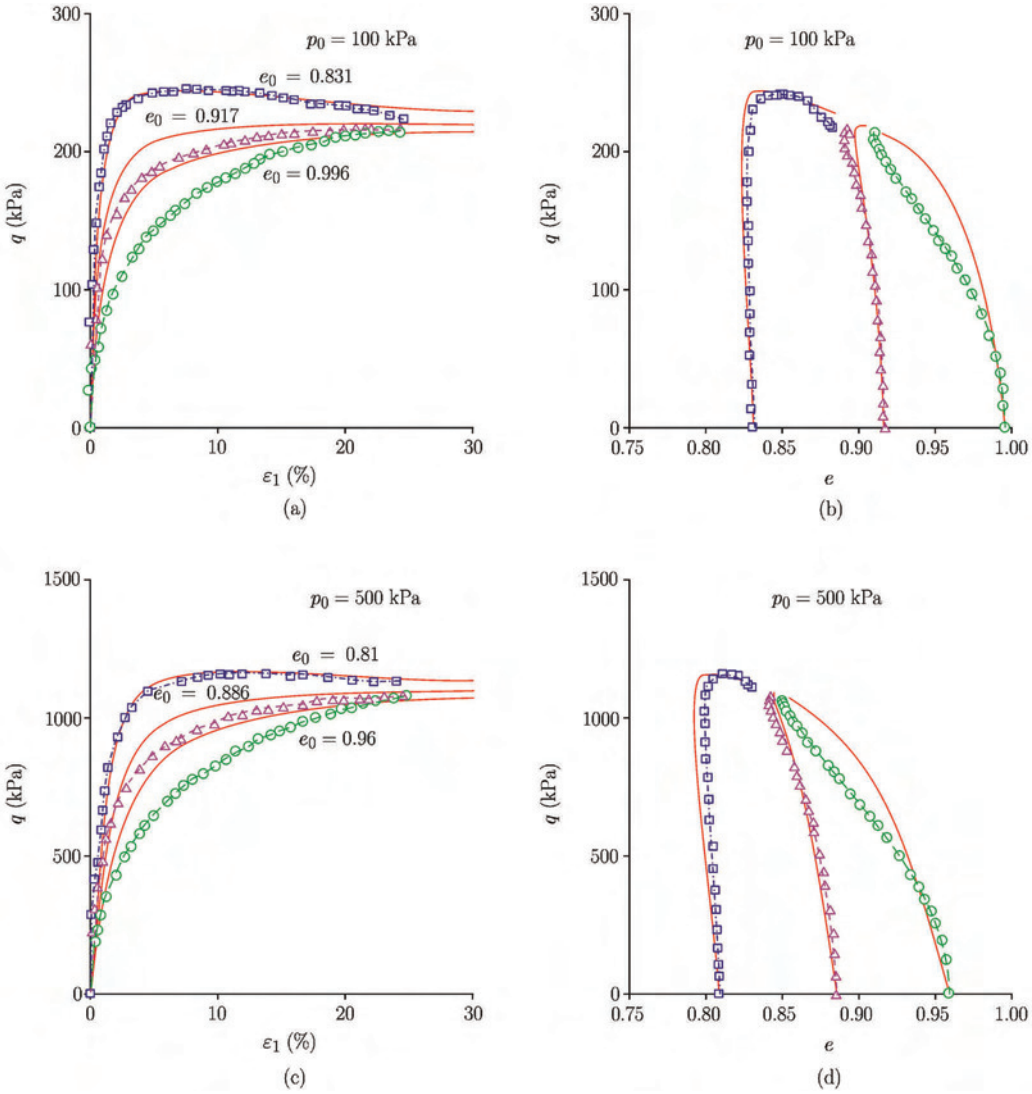

Fig. 9. Comparison between the experimental and numerical results for drained triaxial compression tests of Toyoura sand.

3.4. Cyclic Modeling for Sand

3.4.1. Nevada sand

Cyclic triaxial tests were conducted under undrained loading conditions with different initial confining pressures and densities for the VELACS project[43]. The simulations were conducted using the values of model parameters determined from monotonic tests. In these two undrained cyclic loading cases, the changes in the magnitudes of deviatoric stress are similar, i.e., approximately 30 kPa. As expected, the sample with 40% relative density reached liquefaction in a fewer number of cycles than the sample with 60% relative density for the experimental and simulation results (Fig.14). The proposed model detected the dependence of liquefaction potential on the relative density of sand.

3.4.2. Toyoura sand

Uchida and Stedman[50] conducted cyclic triaxial undrained loading tests to investigate the undrained cyclic behavior of Toyoura sand. In each test, a certain magnitude of cyclic axial strain was applied in each cycle until liquefaction was achieved. The test and prediction results for two samples with 30% and 50% relative densities under initial confining pressures of 400 kPa and 200 kPa subjected to 1% axial strain difference are shown in Figs.15(a) and (b), respectively. The model parameters were calibrated from monotonic tests for the predictions of cyclic tests. In general, the model describes the trend as

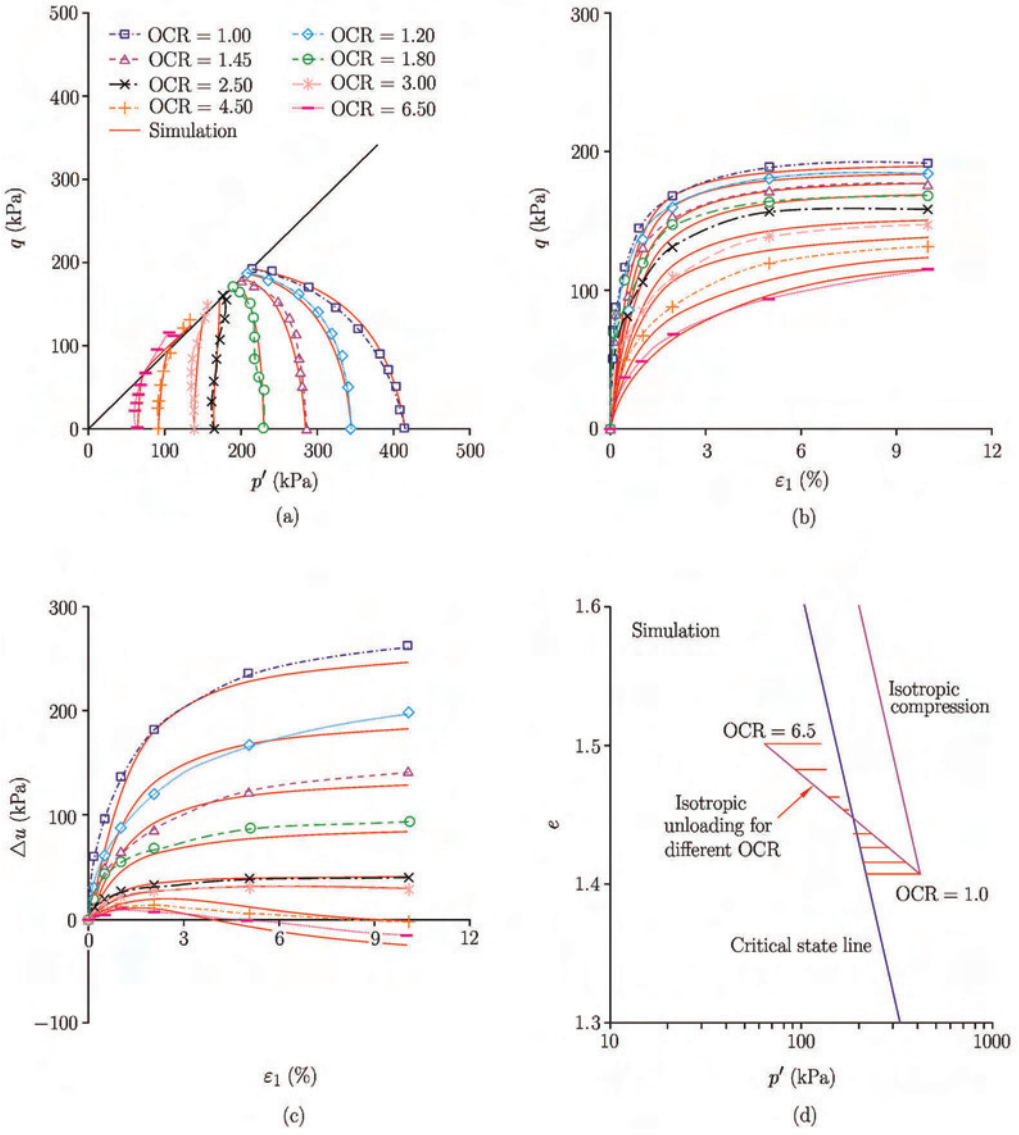

Fig. 10. Comparison between the experimental and numerical results for undrained triaxial tests of pure kaolin clay with OCR from 1 to 6.5.

measured by the test. The fact that looser Toyoura sand under higher confining pressure has a greater liquefaction potential was determined by the model.

Pradhan[51] conducted drained triaxial test under cyclic loading. However, the Toyoura sand used by Pradhan[51] came from a batch different from that used by Verdugo and Ishihara[44]. Thus, the index properties were slightly different. The same values of parameters determined from the tests of Verdugo and Ishihara[44] were used to simulate the drained cyclic test, except $M_c = 1.44$ from the drained test. Despite the difference in the evolution of void ratio between experiments and simulations (Fig.16(c)), which may be attributed to the slight difference in properties among sand from different batches, the proposed model provides a similar trend for the drained cyclic behavior of sand.

3.5. Cyclic Modeling for Clay

3.5.1. Pure clay

Drained triaxial test on speswhite kaolin under cyclic loading conditions was conducted by Al-Tabbaa[52]. Soil was isotropically consolidated to $p'_0 = 300$ kPa, and then loaded cyclically between a stress ratio of 0 and 0.34 at a constant cell pressure. Stress ratio q/p' was plotted against deviatoric

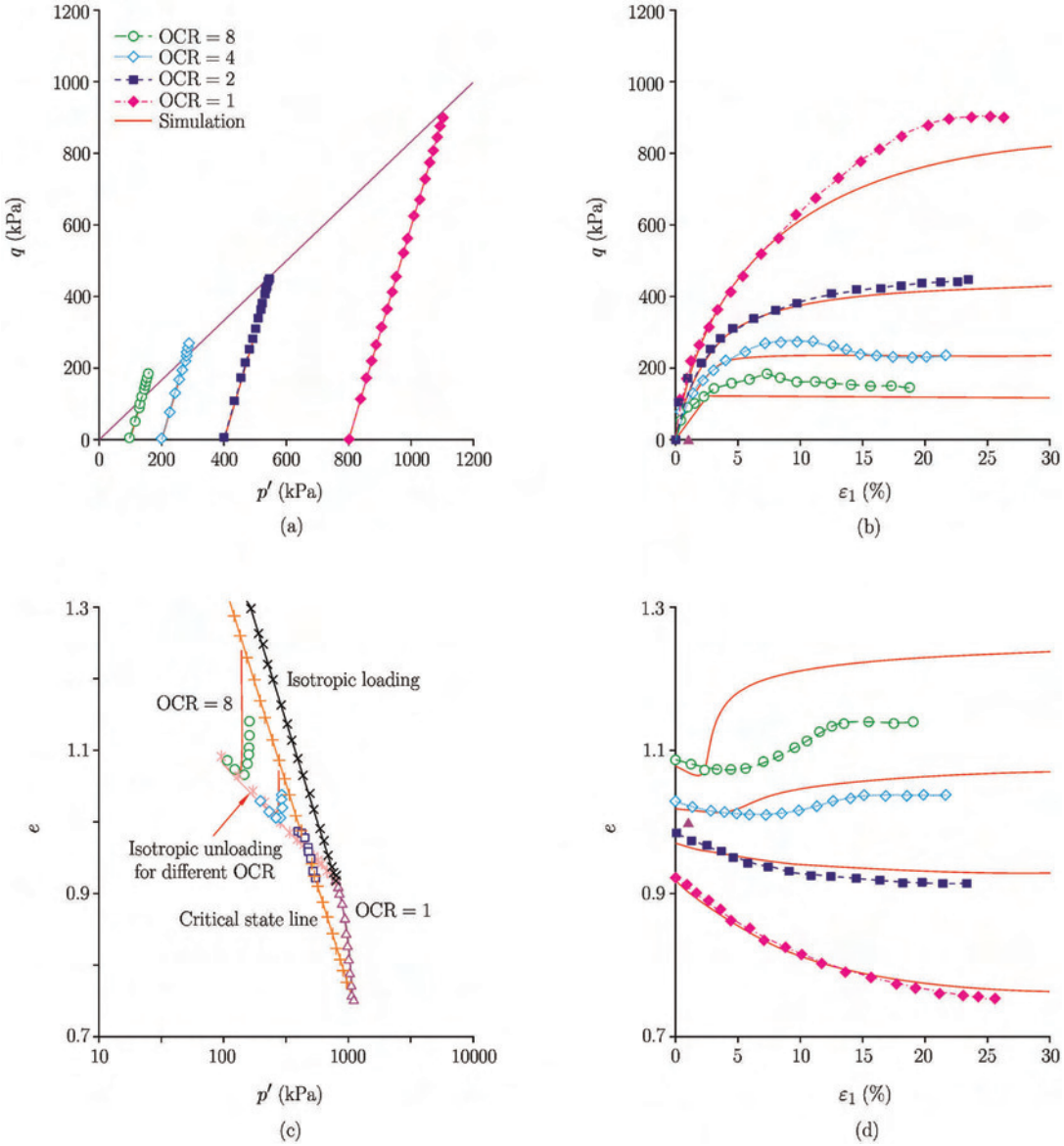

Fig. 11. Comparison between the experimental and numerical results for drained triaxial compression tests of pure black clay with OCR from 1 to 8.

(ε_d) and volumetric (ε_v) strains. Using the elastic and critical state parameters proposed by Stallebrass and Taylor[53] and other parameters determined from the cyclic test, we can conduct a simulation of the drained cyclic test. Figure 17 shows that the same trends of shear and volumetric strains as those from the experimental results were obtained by the proposed model.

3.5.2. Clay mixture

Undrained tests under monotonic and cyclic loadings were conducted by Li and Meissner[42]. Commercially available clay used for landfill lining, ground engineering, and hydraulic structures was adopted in the investigation. The clay mixture has a liquid limit $w_L = 70\%$, a plasticity index $I_p = 45\%$, and a specific gravity of 2.63. The main minerals are kaolinite (60%), illite (5%), and quartz (35%). The samples were consolidated from slurry, which lasted for at least 2 months. The initial void ratio e_0 of the samples varied from 1.0 to 1.15. Conventional triaxial tests were conducted on soil samples that were isotropically reconsolidated with OCR = 1.0, 1.6, and 4.0 for monotonic loading and OCR = 1.0 and 5.1 for cyclic loading. Cyclic loading programs that involved one-way and two-way cyclic tests were

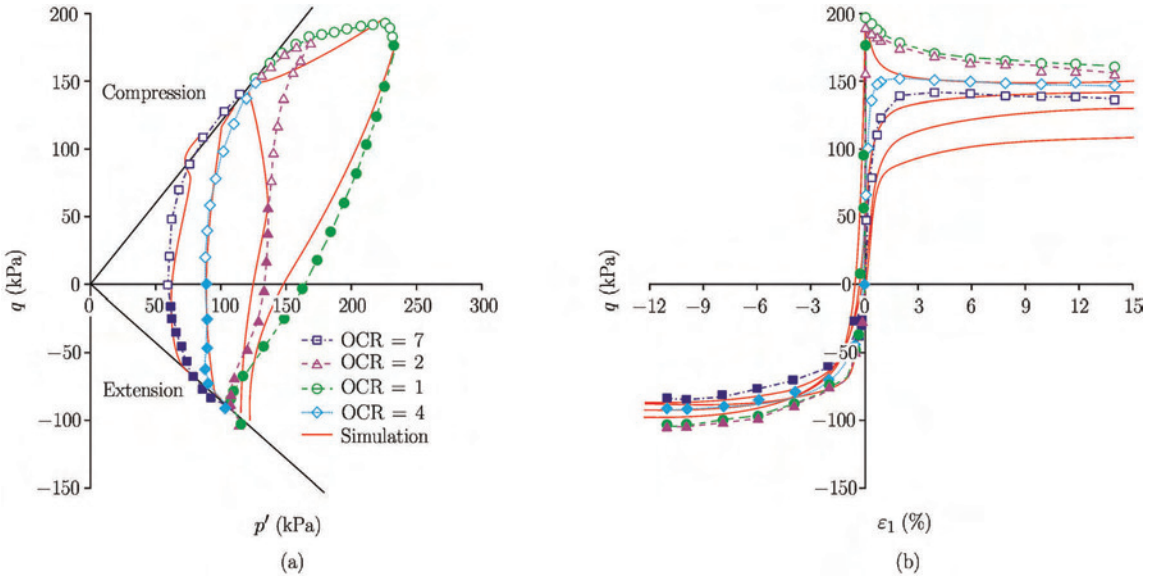

Fig. 12. Comparison between the experimental and numerical results for undrained triaxial compression and extension tests of anisotropically consolidated LCT samples with OCR from 1 to 7.

conducted until steady state or failure was achieved. All cyclic tests were stress controlled using the sinusoidal waveform and a wave frequency of 0.1 Hz. The cyclic stress ratio, which was defined as the ratio of the applied cyclic shear stress to the monotonic shearing strength in compression, ranged from 0.50 to 0.80.

The parameters determined from monotonic tests were used to simulate undrained cyclic tests. Given that the initial slopes of the q-ε_{d} curve for monotonic, one-way, and two-way cyclic tests are different from one another, different values of G_{p0} were selected for each case ($G_{\mathrm{p0}} = 3$ for one-way test, $G_{\mathrm{p0}} = 70$ for two-way test with OCR = 1, and $G_{\mathrm{p0}} = 10$ for two-way test with OCR = 5.1), as conducted by Li and Meissner[42] and Yu et al.[21]. The simulation results for the one-way and two-way cyclic tests are shown in Fig.18 and compared with the experimental results shown in Fig.19. In these figures, the excess pore pressure ($\triangle u$) and deviatoric stress ($\varepsilon_{\mathrm{d}} = \varepsilon_{\mathrm{q}}$) are plotted against the number of cycles and deviatoric strain (q) for samples with OCR = 1 and 5.1, respectively. In general, the proposed model predicts satisfactorily the undrained behavior of clay subjected to one-way and two-way cyclic loading conditions.

IV. CONCLUSION

In this study, we propose a simple and unified modeling method for the monotonic and cyclic behaviors of sand and clay. The proposed model follows the framework of critical state theory and utilizes a Coulomb-type yield surface for shear sliding and another cap-type yield surface for normal compression. The density state is incorporated into the proposed model, which can explicitly consider the locations of the critical state. Plastic hardening modulus and dilatancy relation are dependent on density state, which is different from existing approaches. The shear reversal technique is used to ensure that the model is applicable to various stress paths, including cyclic loading.

The model is used to simulate drained and undrained triaxial tests conducted on various sand and clay types under monotonic and cyclic loading conditions. The prediction results are compared with the experimental results. All simulation results show that the proposed approach is capable of describing the monotonic and cyclic behaviors of sand and clay.

References

[1] Roscoe,K., Schofield,A.N. and Wroth,C., On the yielding of soils. *Géotechnique*, 1958, 8(1): 22-53.
[2] Jefferies,M., Nor-Sand: a simple critical state model for sand. *Géotechnique*, 1993, 43(1): 91-103.
[3] Gajo,A. and Wood,D.M., Severn-Trent sand: a kinematic-hardening constitutive model: the q-p formulation. *Géotechnique*, 1999, 49(5): 595-614.

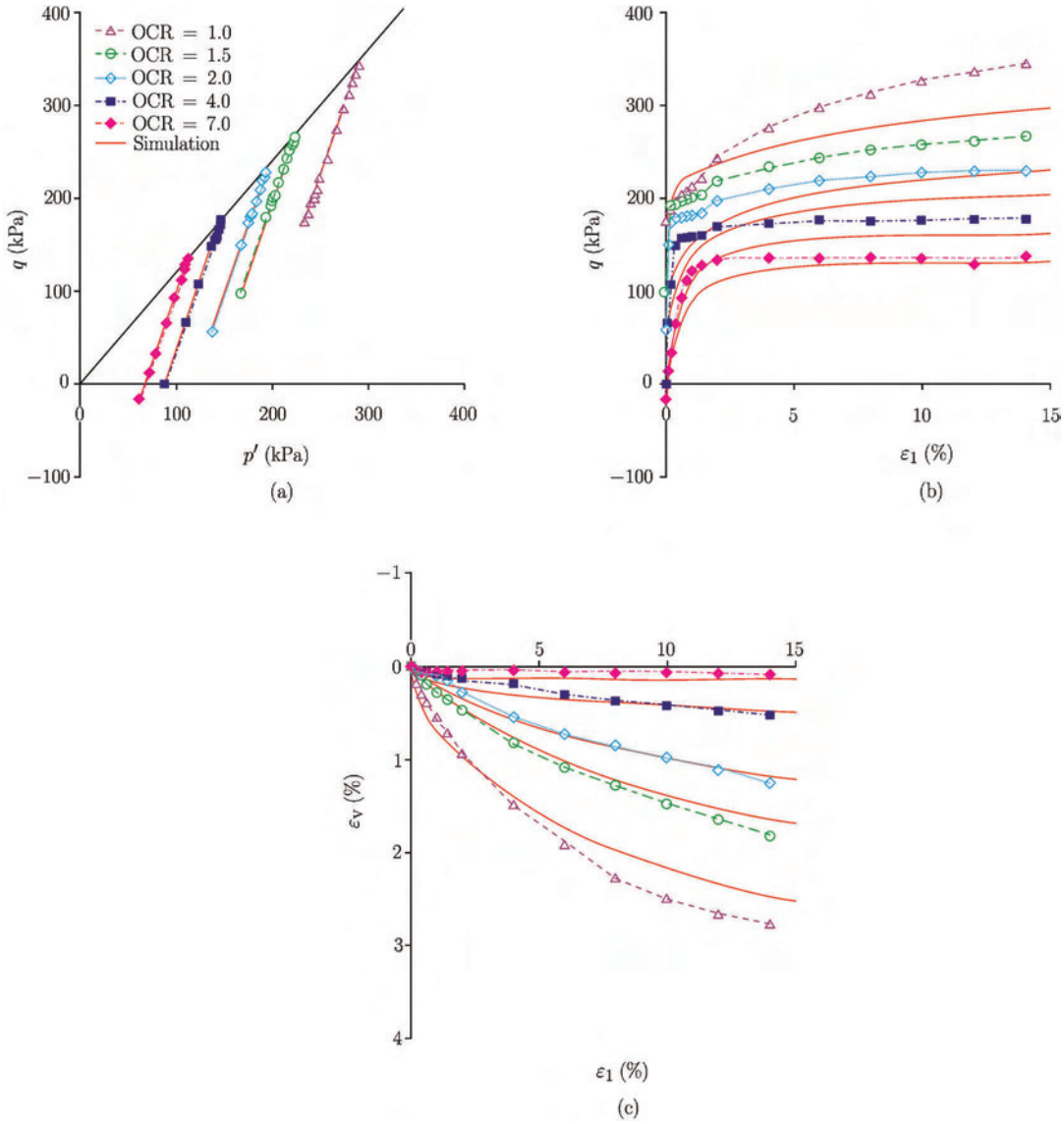

Fig. 13. Comparison between the experimental and numerical results for drained triaxial compression tests of anisotropically consolidated LCT samples with OCR from 1 to 7.

[4] Taiebat,M. and Dafalias,Y.F., SANISAND: simple anisotropic sand plasticity model. *International Journal for Numerical and Analytical Methods in Geomechanics*, 2008, 32(8): 915-948.

[5] Been,K. and Jefferies,M., A state parameter for sands. *Géotechnique*, 1985, 35(2): 990-112.

[6] Wheeler,S.J., Näätänen,A., Karstunen,M., et al., An anisotropic elastoplastic model for soft clays. *Canadian Geotechnical Journal*, 2003, 40(2): 403-418.

[7] Dafalias,Y.F., Manzari,M.T. and Papadimitriou,A.G., SANICLAY: simple anisotropic clay plasticity model. *International Journal for Numerical and Analytical Methods in Geomechanics*, 2006, 30(12): 1231-1257.

[8] Yin,Z.Y. and Hicher,P.Y., Identifying parameters controlling soil delayed behaviour from laboratory and in situ pressuremeter testing. *International Journal for Numerical and Analytical Methods in Geomechanics*, 2008, 32(12): 1515-1535.

[9] Yin,Z.Y., Karstunen,M. and Hicher,P.Y., Evaluation of the influence of elasto-viscoplastic scaling functions on modelling time-dependent behaviour of natural clays. *Soils and Foundations*, 2010, 50(2): 203-214.

[10] Karstunen,M. and Yin,Z.Y., Modelling time-dependent behaviour of Murro test embankment. *Géotechnique*, 2010, 60(10): 735-749.

[11] Yin,Z.Y. and Karstunen,M., Modelling strain-rate-dependency of natural soft clays combined with anisotropy and destructuration. *Acta Mechanica Solida Sinica*, 2011, 24(3): 216-230.

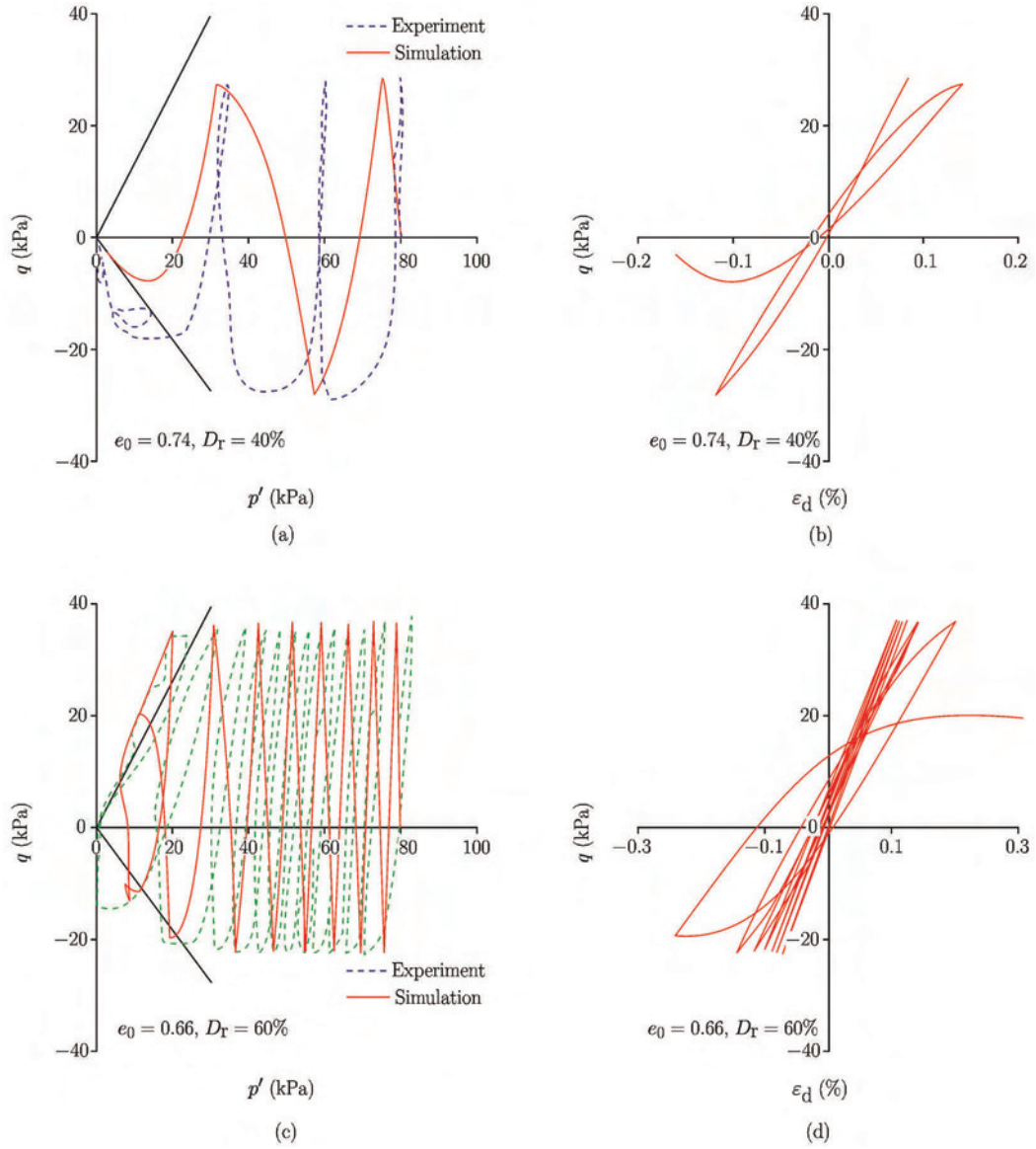

Fig. 14. Comparison between the experimental and numerical results for undrained triaxial tests under cyclic loading of Nevada sand with different densities.

[12] Yin,Z., Karstunen,M., Wang,J., et al., Influence of features of natural soft clay on behaviour of embankment. *Journal of Central South University of Technology*, 2011, 18(5): 1667-1676.

[13] Yin,Z.Y., Chang,C.S., Karstunen,M., et al., An anisotropic elastic-viscoplastic model for soft clays. *International Journal of Solids and Structures*, 2010, 47(5): 665-677.

[14] Yin,Z.Y., Karstunen,M., Chang,C.S., et al., Modeling time-dependent behavior of soft sensitive clay. *Journal of geotechnical and geoenvironmental engineering*, 2011, 137(11): 1103-1113.

[15] Schofield,A.N. and Wroth,P., Critical State Soil Mechanics. Maidenhead: Mcgraw Hill, 1968.

[16] Roscoe,K. and Burland,J., On the generalized stress-strain behaviour of 'wet' clay. In: Engineering Plasticity. Cambridge: Cambridge University Press, 1968: 553-609.

[17] Yu,H., CASM: a unified state parameter model for clay and sand. *International Journal for Numerical and Analytical Methods in Geomechanics*, 1998, 22(8): 621-653.

[18] Pestana,J.M. and Whittle,A.J., Formulation of a unified constitutive model for clays and sands. *International Journal for Numerical and Analytical Methods in Geomechanics*, 1999, 23(12): 1215-1243.

[19] Yao,Y., Sun,D. and Matsuoka,H., A unified constitutive model for both clay and sand with hardening parameter independent on stress path. *Computers and Geotechnics*, 2008, 35(2): 210-222.

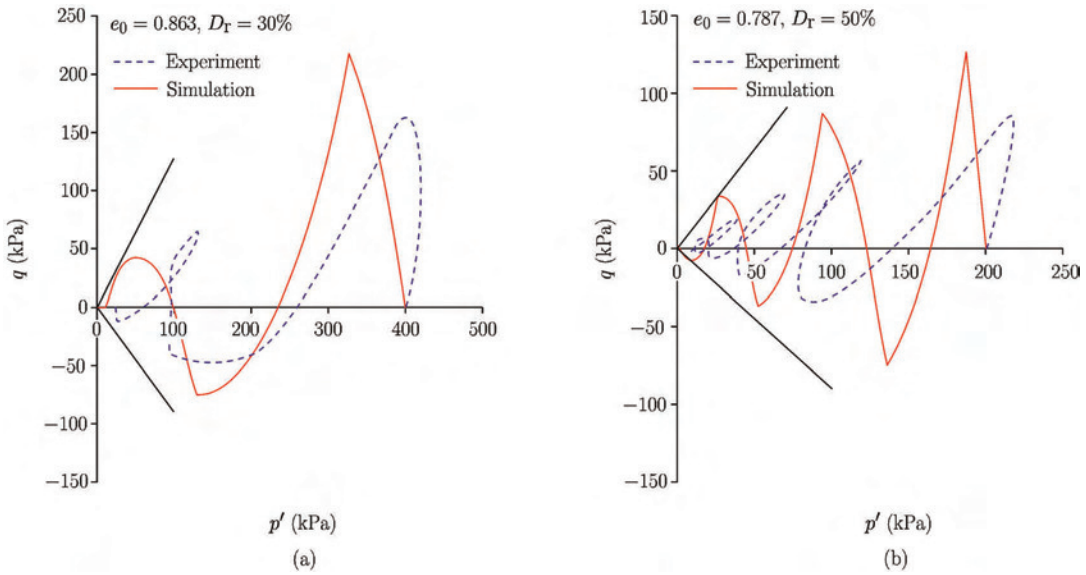

Fig. 15. Comparison between the experimental and numerical results for undrained triaxial tests under cyclic loading of Toyoura sand with different densities.

[20] Pestana,J.M., Whittle,A.J. and Gens,A., Evaluation of a constitutive model for clays and sands: Part II–clay behaviour. *International Journal for Numerical and Analytical Methods in Geomechanics*, 2002, 26(11): 1123-1146.

[21] Yu,H.S., Khong,C. and Wang,J., A unified plasticity model for cyclic behaviour of clay and sand. *Mechanics Research Communications*, 2007, 34(2): 97-114.

[22] Vermeer,P., A double hardening model for sand. *Géotechnique*, 1978, 28(4): 413-433.

[23] Hsieh,H., Kavazanjian,Jr,E. and Borja,R., Double-yield-surface cam-clay plasticity model—I. Theory. *Journal of Geotechnical Engineering*, 1990, 116(9): 1381-1401.

[24] Hu,W., Yin,Z.Y., Dano,C., et al., A constitutive model for granular materials considering grain breakage. *Science China-Technological Sciences*, 2011, 54(8): 2188-2196.

[25] Biarez,J. and Hicher,P.Y., Elementary Mechanics of Soil Behaviour: Saturated Remoulded Soils. AA Balkema, 1994.

[26] Yin,Z.Y., Chang,C.S., Hicher,P.Y., et al., Micromechanical analysis of kinematic hardening in natural clay. *International Journal of Plasticity*, 2009, 25(8): 1413-1435.

[27] Yin,Z.Y. and Chang,C.S., Microstructural modelling of stress-dependent behaviour of clay. *International Journal of Solids and Structures*, 2009, 46(6): 1373-1388.

[28] Yin,Z.Y. and Chang,C.S., Non-uniqueness of critical state line in compression and extension conditions. *International Journal for Numerical and Analytical Methods in Geomechanics*, 2009, 33(10): 1315-1338.

[29] Chang,C.S. and Yin,Z.Y., Modeling stress-dilatancy for sand under compression and extension loading conditions. *Journal of Engineering Mechanics*, 2010, 136(6): 777-786.

[30] Yin,Z.Y., Chang,C.S. and Hicher,P.Y., Micromechanical modelling for effect of inherent anisotropy on cyclic behaviour of sand. *International Journal of Solids and Structures*, 2010, 47(14-15): 1933-1951.

[31] Chang,C.S. and Yin,Z.Y., Micromechanical modeling for inherent anisotropy in granular materials. *Journal of Engineering Mechanics*, 2010, 136(7): 830-839.

[32] Chang,C.S., Yin,Z.Y. and Hicher,P.Y., Micromechanical analysis for interparticle and assembly instability of sand. *Journal of Engineering Mechanics*, 2011, 137(3): 155-168.

[33] Yin,Z.Y., Hattab,M. and Hicher,P.Y., Multiscale modeling of a sensitive marine clay. *International Journal for Numerical and Analytical Methods in Geomechanics*, 2011, 35(15): 1682-1702.

[34] Chang,C.S. and Yin,Z.Y., Micromechanical modeling for behavior of silty sand with influence of fine content. *International Journal of Solids and Structures*, 2011, 48(19): 2655-2667.

[35] Yin,Z.Y., Chang,C.S., Hicher,P.Y., et al., Micromechanical analysis of the behavior of stiff clay. *Acta Mechanica Sinica*, 2011, 27(6): 1013-1022.

[36] Yin,Z.Y. and Chang,C.S., Stress-dilatancy behavior for sand under loading and unloading conditions. *International Journal for Numerical and Analytical Methods in Geomechanics*, 2013, 37(8): 855-870. DOI: 10.1002/nag.1125.

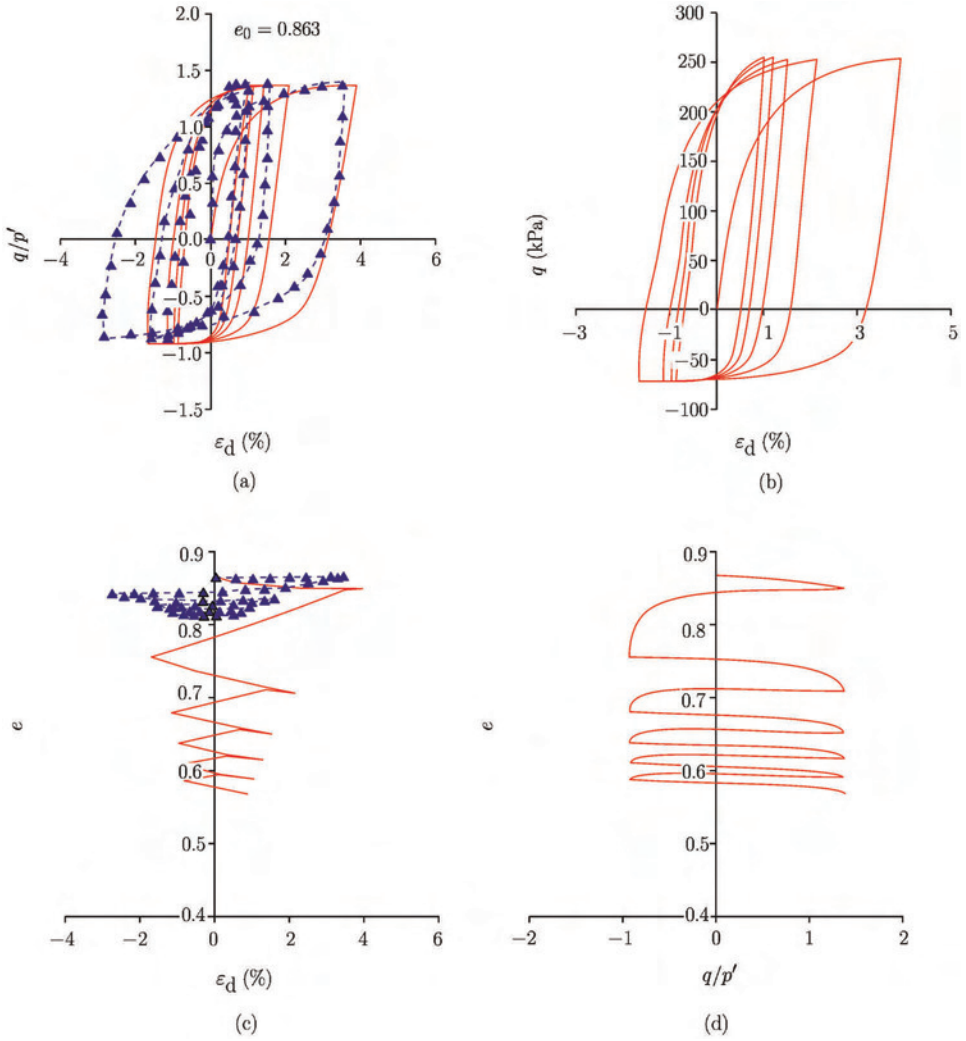

Fig. 16. Comparison between the experimental and numerical results for drained triaxial tests under cyclic loading of Toyoura sand.

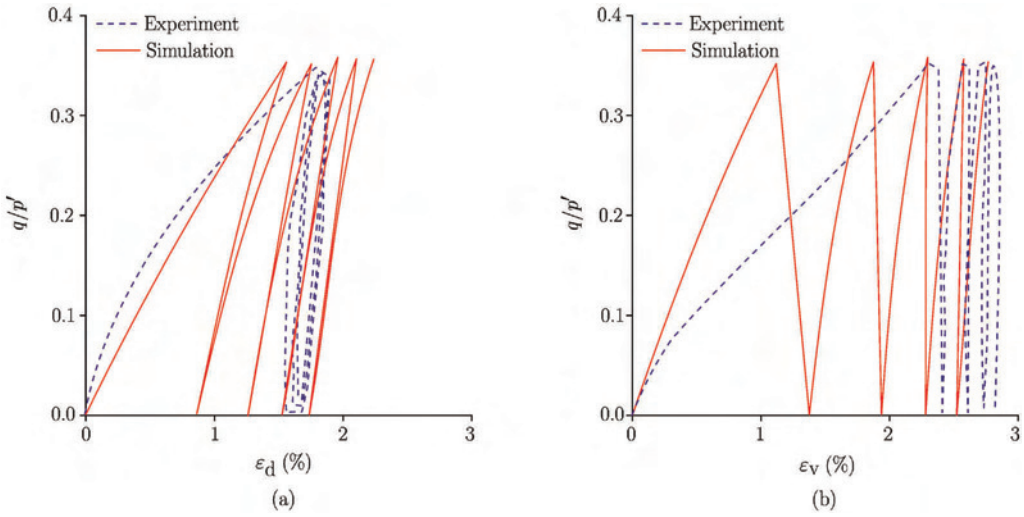

Fig. 17. Comparison between the experimental and numerical results for drained triaxial tests under cyclic loading of kaolin clay (Al-Tabbaa, 1987).

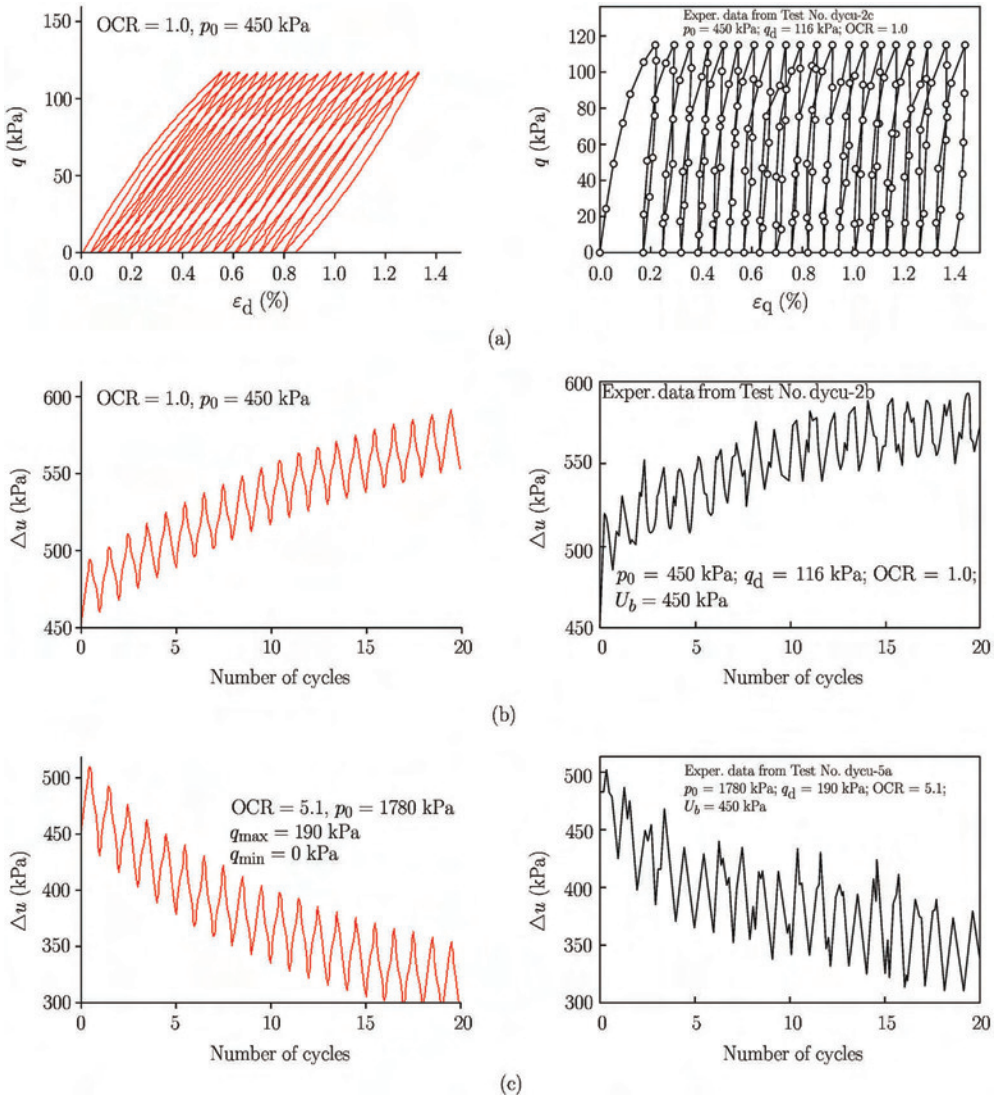

Fig. 18. Comparison between the experimental and numerical results for undrained triaxial tests under one-way cyclic loading of clay mixture (Li and Meissner, 2002).

[37] Yin,Z.Y., Xu,Q. and Chang,C.S., Modeling cyclic behavior of clay by micromechanical approach. *Journal of engineering mechanics*, 2012, doi: 10.1061/(ASCE)EM.1943-7889.0000516.

[38] Sheng,D., Sloan,S. and Yu,H., Aspects of finite element implementation of critical state models. *Computational Mechanics*, 2000, 26(2): 185-196.

[39] Balendran,B. and Nemat-Nasser,S., Double sliding model for cyclic deformation of granular materials, including dilatancy effects. *Journal of the Mechanics and Physics of Solids*, 1993, 41(3): 573-612.

[40] Wan,R.G. and Guo,P.J., Drained cyclic behavior of sand with fabric dependence. *ASCE Journal of Engineering Mechanics*, 2001, 127(11): 1106-1116.

[41] Dafalias,Y. and Herrmann,L., Bounding surface formulation of soil plasticity. In: Pande,G.N. and Zienkiewicz,D.C. (Eds.), Soil Mechanics-Transient and Cyclic Loads. New York: Wiley, 1982, 10: 253-282.

[42] Li,T. and Meissner,H., Two-surface plasticity model for cyclic undrained behavior of clays. *Journal of Geotechnical and Geoenvironmental Engineering*, 2002, 128(7): 613-626.

[43] Arumoli,K., Muraleetharan,K., Hossein,M., et al., VELACS: verification of liquefaction analysis by centrifuge studies–laboratory testing program, soils data report. Technical Report, the Earth Technology Corporation, Irvine, California, 1992.

[44] Verdugo,R. and Ishihara,K., The steady state of sandy soils. *Soils and Foundations*, 1996, 36(2): 81-91.

[45] Miura,N., Murata,H. and Yasufuku,N., Stress-strain characteristics of sand in a particle-crushing region. *Soils and Foundations*, 1984, 24(1): 77-89.

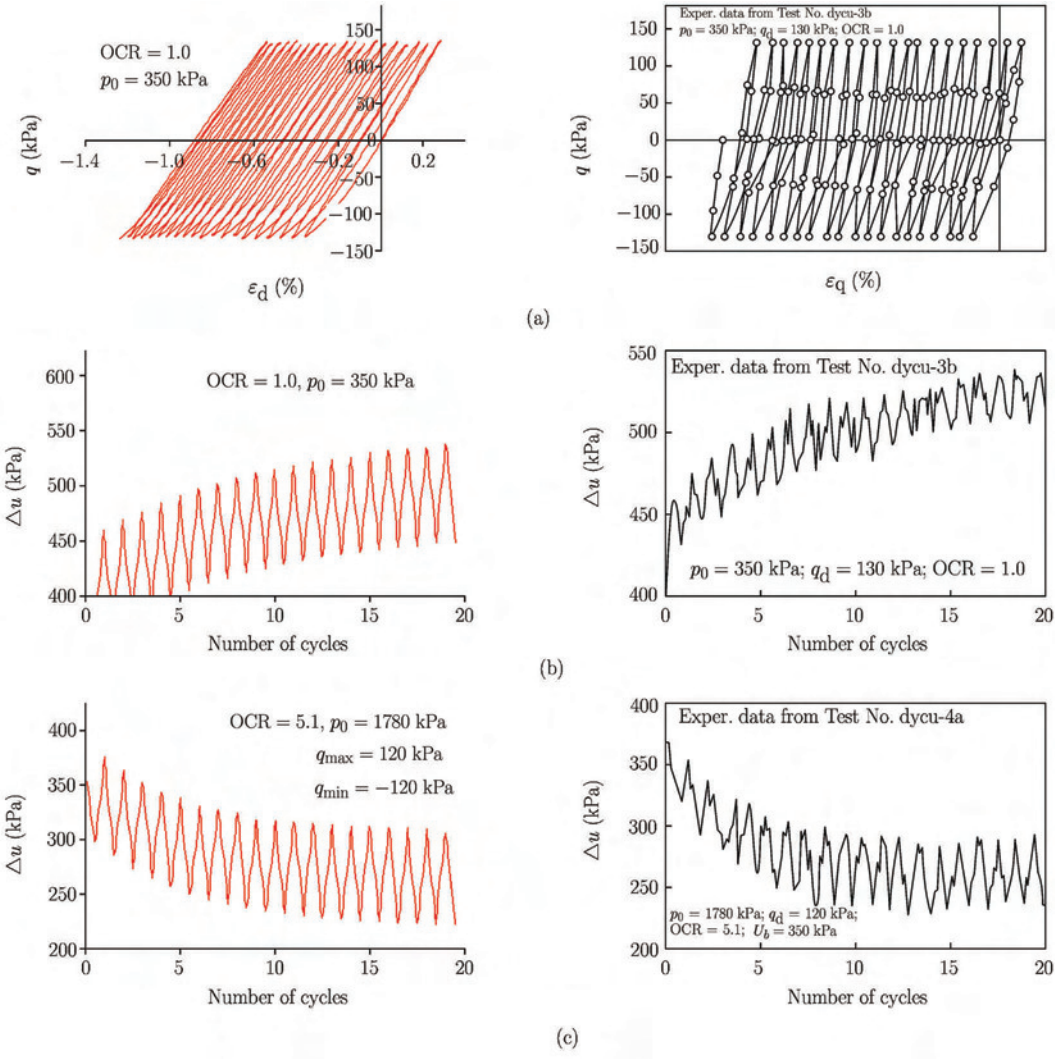

Fig. 19. Comparison between the experimental and numerical results for undrained triaxial tests under two-way cyclic loading of clay mixture (Li and Meissner, 2002).

[46] Miura,N. and Yamanouchi,T., Effect of water on the behavior of a quartz-rich sand under high stresses. *Soils and Foundations*, 1975, 15(4): 23-34.

[47] Yoshimine,M., Ishihara,K. and Vargas,W., Effects of principal stress direction and intermediate principal stress on undrained shear behavior of sand. *Soils and Foundations*, 1998, 38(3): 179-188.

[48] Wroth,C. and Loudon,P., The correlation of strains within a family of triaxial tests on overconsolidated samples of kaolin. *Proc. Geotechn. Conf., Oslo*, 1967, 1: 159-163.

[49] Gens,A., Stress-Strain and Strength of a Low Plasticity Clay. Ph.D. Thesis, Imperial College, London University, 1982.

[50] Uchida,K. and Stedman,J.D., Liquefaction behaviour of Toyoura sand under cyclic strain controlled triaxial loading. Proceedings of the Eleventh International Offshore and Polar Engineering Conference, Stavanger, Norway, 2001: 17-22.

[51] Pradhan,T., The behavior of sand subjected to monotonic and cyclic loadings. Ph.D. Thesis, Japan: Kyoto University, 1989.

[52] Al-Tabbaa,A., Permeability and stress-strain response of speswhite kaolin. Ph.D. Thesis, London: University of Cambridge, 1987.

[53] Stallebrass,S.E. and Taylor,R.N. The development of a constitutive model for the prediction of ground movements in overconsolidated clay. *Géotechnique*, 1997, 47(2): 235-253.